Opto-Electronic Science

Original Article

2022, Vol. 1, No. 3

DOI: 10.29026/oes.2022.210014

Terahertz metasurface zone plates with arbitrary polarizations to a fixed polarization conversion

Zhen Yue[1†], Jitao Li[1†], Jie Li[1†], Chenglong Zheng[1†], Jingyu Liu[2], Guocui Wang[2,3], Hang Xu[1], Mingyang Chen[4], Yating Zhang[1*], Yan Zhang[2*] and Jianquan Yao[1*]

Metasurfaces that can realize the polarization manipulation of electromagnetic waves on the sub-wavelength scale have become an emerging research field. Here, a novel strategy of combining the metasurface and Fresnel zone plate to form a metasurface zone plate is proposed to realize the conversion from nearly arbitrary polarizations to a fixed polarization. Specifically, when one polarized wave is incident on adjacent ring zones constructed by different types of meta-atoms, the transmitted waves generated by odd-numbered and even-numbered ring zones converge at the same focus and superimpose to generate a fixed polarized wave. As function demonstrations, we have designed two types of metasurface zone plates: one is a focused linear polarizer, and the other can convert nearly arbitrary polarized waves into focused circularly polarized waves. The simulated and measured results are consistent with theoretical expectations, suggesting that the proposed concept is flexible and feasible. Our work provides an alternative platform for polarization manipulation and may vigorously promote the development of polarization photonic devices.

Keywords: metasurface zone plates; polarization; conversion; terahertz

Yue Z, Li JT, Li J, Zheng CL, Liu JY et al. Terahertz metasurface zone plates with arbitrary polarizations to a fixed polarization conversion. *Opto-Electron Sci* **1**, 210014 (2022).

Introduction

As an inherent characteristic of electromagnetic waves, polarization has been widely used in many fields such as information processing[1–3], quantum optics[4–6] and polarization imaging[7,8]. Among them, the polarization states of typical electromagnetic waves can be divided into linear polarization, circular polarization and elliptical polarization. For traditional polarization devices, the conversion of arbitrarily polarized waves into the specific polarized wave relies on the combination of linear polarizers and other polarization devices which undoubtedly hinder the development of modern optical devices towards integration and miniaturization.

Recently, the proposal of chiral metamaterials[9–14]

[1]Key Laboratory of Opto-Electronics Information Technology (Tianjin University), Ministry of Education, School of Precision Instruments and Opto-Electronics Engineering, Tianjin University, Tianjin 300072, China; [2]Beijing Key Laboratory for Metamaterials and Devices, Department of Physics, Capital Normal University, Beijing 100048, China; [3]Beijing Engineering Research Center for Mixed Reality and Advanced Display, School of Optics and Photonics, Beijing Institute of Technology, Beijing 100081, China; [4]Department of Optoelectronic Information Science and Engineering, Jiangsu University, Zhenjiang 212013, China.

[†]These authors contributed equally to this work.

[*]Correspondence: YT Zhang, E-mail: yating@tju.edu.cn; Y Zhang, E-mail: yzhang@cnu.edu.cn; JQ Yao, E-mail: jqyao@tju.edu.cn

Received: 19 December 2021; Accepted: 16 February 2022; Published online: 18 March 2022

which can be constructed from chiral atoms with strong circular dichroism, has provided another option for realizing the polarization conversion from non-polarized waves to circularly polarized (CP) waves. However, limited by processing accuracy and manufacturing cost, chiral metamaterials are not conducive to further promoting the development of circular polarizers. With this, the in-plane chiral structures[15–21] were proposed to construct planar chiral metamaterials, also called chiral metasurfaces, to reduce the size of devices. Various chiral structures with strong circular dichroism have been investigated, such as L-type[22], Z-type[23,24], H-type[25], asymmetric split ring[26,27] and fish-scale[28].

In parallel, different from the above-mentioned metasurfaces based on chiral meta-atoms, the metasurfaces formed by combining several anisotropic meta-atoms can also achieve circular asymmetric transmission[29–32]. For example, two pair meta-atoms with a specific rotation angle difference are utilized as a cell to form a metasurface, and beam interference is applied to make left-handed circularly polarized (LCP) waves incident only generate right-handed circularly polarized (RCP) waves, nevertheless the metasurface do not engender outgoing wave under RCP incidence[30]. Besides, linearly polarized (LP) waves also play an important role in high-resolution imaging. In recent years, metasurface linear polarizers that do not rely on external analyzers to directly observe high-resolution imaging have been reported[33–35]. For example, by utilizing a double-layer metasurface composed of aluminum nanorods, a full-broadband polarization-selective transmission of light waves in the near-infrared band has been realized[33]. Moreover, by independently tailoring the direction angle of each nanorod, nearly arbitrary intensity manipulation of LP beam could be obtained, which could provide another option for imaging or information encoding.

Therefore, circular and linear polarizers relying on metasurfaces efficiently realize polarization manipulation on the sub-wavelength scale. Certainly, metasurfaces that can control the wavefront while realizing polarization manipulation are more attractive. Here, we introduce the Fresnel zone plate into the metasurface to construct the metasurface zone plate[36–38] with focusing function to generate LP or CP wave. For metasurface zone plates, the odd-numbered and even-numbered ring zones are composed of different meta-atoms and the total number of rings is even. Then, once one polarized beam is incident, the outgoing waves in response to the odd-numbered and the even-numbered ring zones are focused on the same point and superimposed to engender a fixed polarized wave. As shown in Fig. 1(a) and 1(b), when the unpolarized beam is incident, the outgoing beams generated are *x*-LP and RCP, respectively. Such a strategy provides a novel platform for the design of multifunctional polarized metasurfaces and is expected to promote the development of optical devices towards miniaturization and integration.

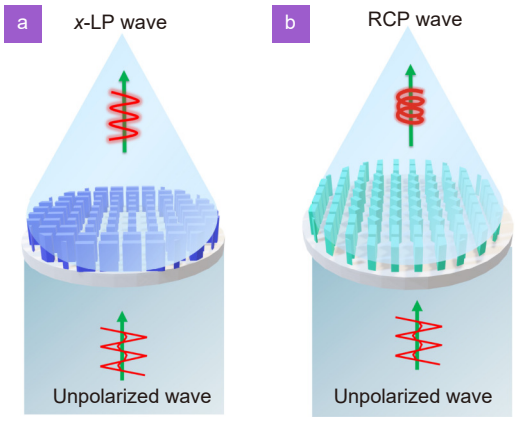

Fig. 1 | (**a**) Performing diagram of *x*-LP beam generator. (**b**) Schematic diagram of RCP beam generation under non-polarized incidence.

Results and discussion

Principle

Here, to realize the polarization conversion from nearly arbitrary polarizations to a fixed polarization, metasurface zone plates are proposed. Compared with the traditional zone plates, each ring in the metasurface zone plates is composed of micro-structured dielectric pillars to realize the independent manipulation of the polarization, phase and amplitude, which empowers the zone plates diversified functions. For one metasurface zone plate, the outer radius of the nth ring can be expressed as (see Supplementary information Section 1 for details):

$$r_n = \sqrt{nf\lambda_0}\left(1+\frac{n\lambda_0}{4f}\right)^{1/2}, \tag{1}$$

where λ_0 = 300 μm is the performing wavelength, f =1.7 mm is the focal length corresponding to λ_0, and n represents a positive integer. When the metasurface zone plate meets the following conditions: all the meta-atoms constituting the ring zone are the same, and the number of rings n is less than 20 and greater than 2, the complex amplitude at the focus is (see Supplementary

information Section 1 for details):

$$\boldsymbol{E}=\sum_{j=1}^{n}\boldsymbol{E}_j\approx\begin{cases}m\left|\boldsymbol{E}_1\right|+\mathrm{e}^{\mathrm{i}\pi}\left(m-1\right)\left|\boldsymbol{E}_1\right|, n=2m-1\\ m\left|\boldsymbol{E}_1\right|+\mathrm{e}^{\mathrm{i}\pi}m\left|\boldsymbol{E}_1\right|, \quad n=2m\end{cases}, \tag{2}$$

where m is a positive integer greater than 1. It is worth noting that when n is an even number, the absolute values of the complex amplitudes generated by the odd-numbered and the even-numbered ring zones at the focus are practically equal.

Next, we discuss the case where the odd-numbered and the even-numbered rings are composed of different meta-atoms, and n is an even number. Assuming that the incident beam $\boldsymbol{E}_{\rm in}$ with an amplitude of 1 can be expressed as:

$$\boldsymbol{E}_{\rm in}=\begin{bmatrix}A\\B\end{bmatrix}=A\begin{bmatrix}1\\0\end{bmatrix}+B\begin{bmatrix}0\\1\end{bmatrix}, \left|A\right|^2+\left|B\right|^2=1, \tag{3}$$

where A and B stand for arbitrary complex numbers. In the Cartesian coordinate system, the Eq. (3) can be rewritten as:

$$\boldsymbol{E}_{\rm in}=\frac{A+\mathrm{i}B}{2}\begin{bmatrix}1\\-\mathrm{i}\end{bmatrix}+\frac{A-\mathrm{i}B}{2}\begin{bmatrix}1\\\mathrm{i}\end{bmatrix}. \tag{4}$$

In recent years, coupled mode theory (CMT) has been used to study the relevant properties of transmission metasurfaces[39–42], which further promotes the development of metasurfaces. Here, only the polarization conversion properties of metasurfaces are considered to be studied from the Jones matrix. For a lossless anisotropic meta-atom, the corresponding Jones matrix is:

$$\mathbf{J}=\boldsymbol{R}^{\rm T}\begin{bmatrix}\mathrm{e}^{\mathrm{i}\varphi_x}&0\\0&\mathrm{e}^{\mathrm{i}\varphi_y}\end{bmatrix}\boldsymbol{R}, \tag{5}$$

where $\boldsymbol{R}$ is the rotation matrix with the rotation angle θ, φ_x (φ_y) represents the phase delay propagating along the x (y) direction under x-LP (y-LP) incidence. We set the Jones matrix of the even-numbered zone as $\mathbf{J}_1$ and the Jones matrix of the odd-numbered zone as $\mathbf{J}_2$, then the following transmitted electric field at the focus can be obtained according to Eq. (2) (see Supplementary information Section 2 for details):

$$\begin{aligned}\boldsymbol{E}_{\rm oute}&=\boldsymbol{E}_{\rm in}\cdot\mathbf{J}_1=\left(\frac{A+\mathrm{i}B}{2}\begin{bmatrix}1\\-\mathrm{i}\end{bmatrix}+\frac{A-\mathrm{i}B}{2}\begin{bmatrix}1\\\mathrm{i}\end{bmatrix}\right)\cdot\boldsymbol{R}_1^{\rm T}\begin{bmatrix}\mathrm{e}^{\mathrm{i}\varphi_{x1}}&0\\0&\mathrm{e}^{\mathrm{i}\varphi_{y1}}\end{bmatrix}\boldsymbol{R}_1\\&=\left[\frac{A-\mathrm{i}B}{4}\cdot\cos\left(\frac{\Delta\varphi_1}{2}\right)\cdot\mathrm{e}^{\mathrm{i}\frac{\sum\varphi_1}{2}}+\frac{A+\mathrm{i}B}{4}\cdot\sin\left(\frac{\Delta\varphi_1}{2}\right)\cdot\mathrm{e}^{\mathrm{i}\left(\frac{\sum\varphi_1}{2}-\frac{\pi}{2}-2\theta_1\right)}\right]\cdot\begin{bmatrix}1\\\mathrm{i}\end{bmatrix}\\&+\left[\frac{A-\mathrm{i}B}{4}\cdot\sin\left(\frac{\Delta\varphi_1}{2}\right)\cdot\mathrm{e}^{\mathrm{i}\left(\frac{\sum\varphi_1}{2}-\frac{\pi}{2}+2\theta_1\right)}+\frac{A+\mathrm{i}B}{4}\cos\left(\frac{\Delta\varphi_1}{2}\right)\cdot\mathrm{e}^{\mathrm{i}\frac{\sum\varphi_1}{2}}\right]\cdot\begin{bmatrix}1\\-\mathrm{i}\end{bmatrix}\\\boldsymbol{E}_{\rm outo}&=\boldsymbol{E}_{\rm in}\cdot\mathbf{J}_2=\left(\frac{A+\mathrm{i}B}{2}\begin{bmatrix}1\\-\mathrm{i}\end{bmatrix}+\frac{A-\mathrm{i}B}{2}\begin{bmatrix}1\\\mathrm{i}\end{bmatrix}\right)\cdot\boldsymbol{R}_2^{\rm T}\begin{bmatrix}\mathrm{e}^{\mathrm{i}\varphi_{x2}}&0\\0&\mathrm{e}^{\mathrm{i}\varphi_{y2}}\end{bmatrix}\boldsymbol{R}_2\\&=\left[\frac{\mathrm{i}B-A}{4}\cdot\cos\left(\frac{\Delta\varphi_2}{2}\right)\cdot\mathrm{e}^{\mathrm{i}\frac{\sum\varphi_2}{2}}-\frac{A+\mathrm{i}B}{4}\cdot\sin\left(\frac{\Delta\varphi_2}{2}\right)\cdot\mathrm{e}^{\mathrm{i}\left(\frac{\sum\varphi_2}{2}-\frac{\pi}{2}-2\theta_2\right)}\right]\cdot\begin{bmatrix}1\\\mathrm{i}\end{bmatrix}\\&+\left[\frac{\mathrm{i}B-A}{4}\cdot\sin\left(\frac{\Delta\varphi_2}{2}\right)\cdot\mathrm{e}^{\mathrm{i}\left(\frac{\sum\varphi_2}{2}-\frac{\pi}{2}+2\theta_2\right)}-\frac{A+\mathrm{i}B}{4}\cos\left(\frac{\Delta\varphi_2}{2}\right)\cdot\mathrm{e}^{\mathrm{i}\frac{\sum\varphi_2}{2}}\right]\cdot\begin{bmatrix}1\\-\mathrm{i}\end{bmatrix},\end{aligned} \tag{6}$$

where $\boldsymbol{E}_{\rm oute}$ ($\boldsymbol{E}_{\rm outo}$) is the transmitted electric field generated by the even-numbered (odd-numbered) ring zones at the focus, φ_{x1} and φ_{y1} are the corresponding phase delays along the x and y axes in the even-numbered ring zones, φ_{x2} and φ_{y2} are the corresponding phase delays in the odd-numbered ring zones, and θ_1 (θ_2) represents the rotation angle of the meta-atom in the even-numbered (odd-numbered) ring zones. Besides, the phase summations and differences corresponding to the meta-atoms can be defined as: $\Sigma\varphi_1=\varphi_{x1}+\varphi_{y1}$, $\Delta\varphi_1=\varphi_{x1}-\varphi_{y1}$, $\Sigma\varphi_2=\varphi_{x2}+\varphi_{y2}$, and $\Delta\varphi_2=\varphi_{x2}-\varphi_{y2}$.

Linear polarizer with focusing function

In order to convert the incident arbitrary polarization into linear polarization, the phase difference corresponding to the meta-atom in the odd-numbered ring zones is 0, while the phase difference responses to two orthogonal linear polarizations in the even-numbered ring zones is –π. Therefore, Eq. (6) can be rewritten as:

$$\begin{cases}\boldsymbol{E}_{\rm oute}=-\dfrac{A-\mathrm{i}B}{4}\cdot\mathrm{e}^{\mathrm{i}\left(\varphi_{x1}+2\theta_1\right)}\cdot\begin{bmatrix}1\\-\mathrm{i}\end{bmatrix}\\\qquad\quad-\dfrac{A+\mathrm{i}B}{4}\cdot\mathrm{e}^{\mathrm{i}\left(\varphi_{x1}-2\theta_1\right)}\cdot\begin{bmatrix}1\\\mathrm{i}\end{bmatrix}\\\boldsymbol{E}_{\rm outo}=\dfrac{\mathrm{i}B-A}{4}\cdot\mathrm{e}^{\mathrm{i}\varphi_{x2}}\cdot\begin{bmatrix}1\\\mathrm{i}\end{bmatrix}-\dfrac{A+\mathrm{i}B}{4}\mathrm{e}^{\mathrm{i}\varphi_{x2}}\cdot\begin{bmatrix}1\\-\mathrm{i}\end{bmatrix}\end{cases}. \tag{7}$$

Then, the electric field of the transmitted wave on the focal plane is:

$$\begin{aligned}\boldsymbol{E}_{\rm out}=&\left[-\frac{A-\mathrm{i}B}{4}\cdot\mathrm{e}^{\mathrm{i}\left(\varphi_{x1}+2\theta_1\right)}-\frac{A+\mathrm{i}B}{4}\mathrm{e}^{\mathrm{i}\varphi_{x2}}\right]\cdot\begin{bmatrix}1\\-\mathrm{i}\end{bmatrix}\\&+\left[\frac{\mathrm{i}B-A}{4}\cdot\mathrm{e}^{\mathrm{i}\varphi_{x2}}-\frac{A+\mathrm{i}B}{4}\cdot\mathrm{e}^{\mathrm{i}\left(\varphi_{x1}-2\theta_1\right)}\right]\cdot\begin{bmatrix}1\\\mathrm{i}\end{bmatrix}.\end{aligned} \tag{8}$$

When Eq. (8) satisfies the following conditions: $\varphi_{x1} = \pi$, $\varphi_{x2} = 0$, we can get:

$$\begin{aligned}\boldsymbol{E}_{\text{out}} &= \left[\frac{A-\mathrm{i}B}{4}\mathrm{e}^{\mathrm{i}2\theta_1} - \frac{A+\mathrm{i}B}{4}\right]\cdot\begin{bmatrix}1\\-\mathrm{i}\end{bmatrix} \\ &+ \left[\frac{\mathrm{i}B-A}{4} + \frac{A+\mathrm{i}B}{4}\mathrm{e}^{-\mathrm{i}2\theta_1}\right]\cdot\begin{bmatrix}1\\\mathrm{i}\end{bmatrix} \\ &= (-A\sin\theta_1 + B\cos\theta_1)\begin{bmatrix}\sin\theta_1\\-\cos\theta_1\end{bmatrix}. \end{aligned} \tag{9}$$

According to Eq. (9), it can be determined that the outgoing wave on the focal plane is the LP wave related to θ_1. Since θ_2 does not affect the result, the metasurface zone plate can be rotated at an arbitrary angle along the optical axis to generate a corresponding LP wave on the focal plane. For example, substitute $\theta_1 = \pi/2$ into Eq. (9):

$$\boldsymbol{E}_{\text{out}} = \left(-A\sin\frac{\pi}{2} + B\cos\frac{\pi}{2}\right)\begin{bmatrix}\sin\frac{\pi}{2}\\-\cos\frac{\pi}{2}\end{bmatrix} = -A\begin{bmatrix}1\\0\end{bmatrix}. \tag{10}$$

Surprisingly, as long as A is not equal to 0, the polarization state of the transmitted wave on the focal plane remains x-linear polarization. Specifically, as long as the incident polarized wave is not a y-LP wave, the wave generated by the metasurface zone plate only exists an x-LP component on the focusing plane.

To further verify the correctness of the above results, CST microwave studio is utilized to construct and determine the required all-silicon meta-atoms with dielectric constant ε = 11.9. After parameter scanning, the structure diagram shown in Fig. 2(a) is obtained. The period of all the meta-atoms constituting the metasurface zone plate is P = 150 μm, the length and width of the dielectric pillars in the even-numbered ring zones are L_1 = 50 μm and W_1 = 120 μm, and the length and width of the other dielectric pillars in the odd-numbered ring zones are L_2 = 60 μm and W_2 = 60 μm (see Supplementary information Section 3 for details). In order to obtain the designed metasurface zone plate (see Fig. 2(a)), these two meta-atoms are arranged according to Eq. (1). Figure 2(b) illustrates the intensity distributions of the x-LP and y-LP components of the exit wave on the xz plane under x-LP incidence. It can be seen that the x-LP component is focused on a point, while the intensity of the y-LP component at this point is negligible, indicating that the metasurface zone plate generates x-LP waves on the focal plane under the incidence of x-LP wave. Figure 2(c) depicts the simulated results on the x-o-z plane under y-LP illumination, which are consistent with the above theoretical results. Figure 2(d) shows the intensity profiles on the focal plane at a distance of 1.7 mm from the metasurface zone plate under the incidences of LP, CP and elliptically polarized (EP) waves. It is worth noting that under y-LP incidence, the metasurface zone plate cannot generate the electromagnetic wave on the focal

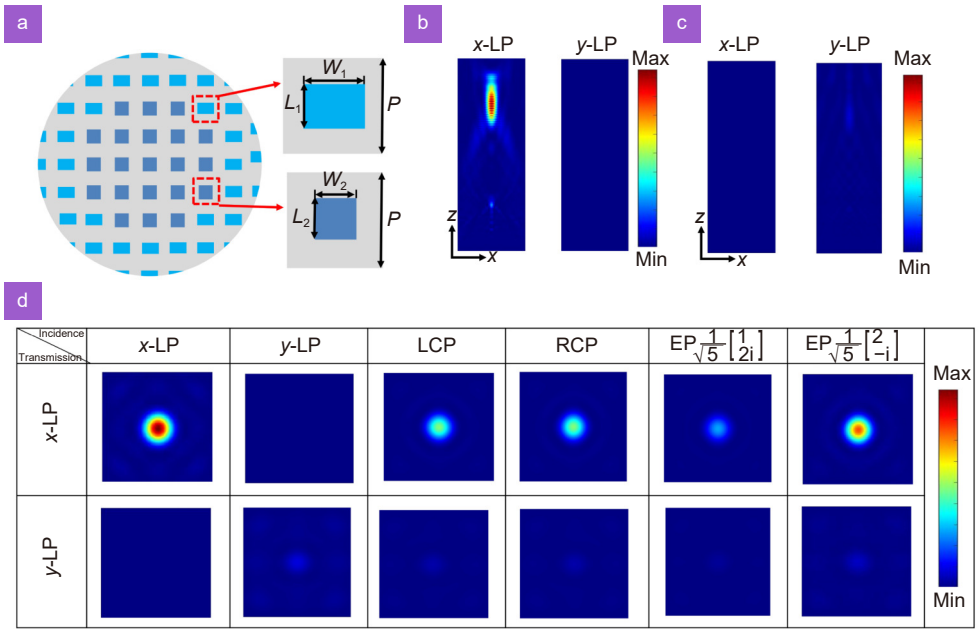

Fig. 2 | (**a**) Schematic diagram of the linear polarizer. (**b**) Simulated results on the xz plane under x-LP incidence. (**c**) The intensity distributions of the transmitted x-LP and y-LP components on the xz plane under y-LP illumination. (**d**) The intensity profiles of the orthogonal LP components of the outgoing wave at the focal plane, under different polarized incidences.

plane, while under the incidences of other polarized waves, the transmitted waves possess only *x*-LP components on the focusing plane. In addition, it can be concluded that under the incidence of *x*-LP waves, the corresponding polarization conversion ratio of the focal plane is close to 100%. Meanwhile, the polarization conversion ratio under the CP incidence is close to 50%. That is to say, the more *x*-LP components occupied in the incident polarized wave, the greater the polarization conversion efficiency of the *x*-LP wave generated by the metasurface zone plate.

The sample with a size of 1.4 mm ×1.4 mm is fabricated exploiting standard UV lithography and inductively coupled plasma (ICP) etching techniques, whose scanning electron microscopy (SEM) image is illustrated in Fig. 3(a). The sample is placed in a terahertz digital holographic imaging system to characterize its optical properties. By introducing a half-wave plate, the polarization state of the probe beam can be changed, and then the two-dimensional terahertz field distribution of the corresponding polarization state can be obtained. Figure 3(b) shows the measured intensity distributions of LP waves under LP incidences, indicating that the designed metasurface zone plate is a linear polarizer with focusing characteristics.

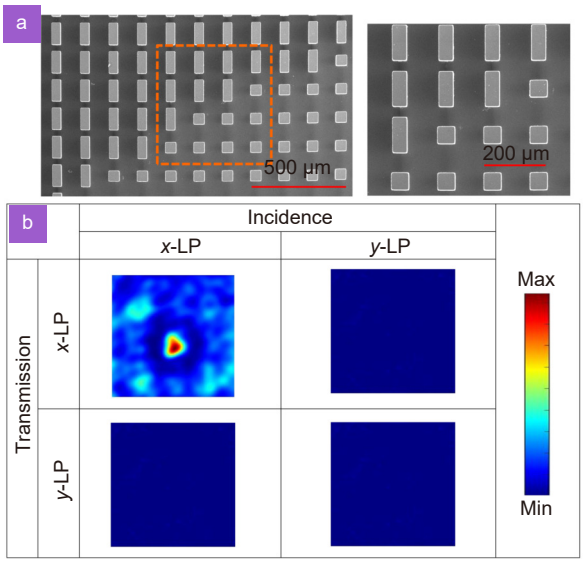

Fig. 3 | (**a**) SEM image of the sample. (**b**) The measured intensity profiles of *x*-LP and *y*-LP components on the focal plane, under the incidences of four polarized waves.

The CP conversion dichroism metasurface zone plate

By introducing two kinds of meta-atoms with a phase difference of π to construct the other metasurface zone plate, it can convert incident polarized waves into a focused CP wave. Thus, substituting $\Delta\varphi_1 = \Delta\varphi_2 = \pi$ into Eq. (6) can be simplified to:

$$\begin{cases} \boldsymbol{E}_{\text{oute}} = -\dfrac{A+\mathrm{i}B}{4}\cdot \mathrm{e}^{\mathrm{i}\left(\varphi_{x1}-2\theta_1\right)}\cdot\begin{bmatrix}1\\ \mathrm{i}\end{bmatrix} + \dfrac{\mathrm{i}B-A}{4}\cdot \mathrm{e}^{\mathrm{i}\left(\varphi_{x1}+2\theta_1\right)}\cdot\begin{bmatrix}1\\ -\mathrm{i}\end{bmatrix} = G\cdot\begin{bmatrix}1\\ \mathrm{i}\end{bmatrix} + H\cdot\begin{bmatrix}1\\ -\mathrm{i}\end{bmatrix} \\ \boldsymbol{E}_{\text{outo}} = \dfrac{A+\mathrm{i}B}{4}\cdot \mathrm{e}^{\mathrm{i}\left(\varphi_{x2}-2\theta_2\right)}\cdot\begin{bmatrix}1\\ \mathrm{i}\end{bmatrix} + \dfrac{A-\mathrm{i}B}{4}\cdot \mathrm{e}^{\mathrm{i}\left(\varphi_{x2}+2\theta_2\right)}\cdot\begin{bmatrix}1\\ -\mathrm{i}\end{bmatrix} = I\cdot\begin{bmatrix}1\\ \mathrm{i}\end{bmatrix} + J\cdot\begin{bmatrix}1\\ -\mathrm{i}\end{bmatrix} \end{cases}. \tag{11}$$

According to Eq. (11), to generate only CP wave at the focal plane, the following conditions need to satisfy:

$$\begin{cases} G-I = -\dfrac{A+\mathrm{i}B}{4}\cdot\left[\mathrm{e}^{\mathrm{i}\left(\varphi_{x1}-2\theta_1\right)} + \mathrm{e}^{\mathrm{i}\left(\varphi_{x2}-2\theta_2\right)}\right] \equiv 0 \\ H+J = \dfrac{\mathrm{i}B-A}{4}\cdot\left[\mathrm{e}^{\mathrm{i}\left(\varphi_{x1}+2\theta_1\right)} - \mathrm{e}^{\mathrm{i}\left(\varphi_{x2}+2\theta_2\right)}\right] \equiv 0 \end{cases}, \tag{12}$$

$$\begin{cases} G+I = -\dfrac{A+\mathrm{i}B}{4}\cdot\left[\mathrm{e}^{\mathrm{i}\left(\varphi_{x1}-2\theta_1\right)} - \mathrm{e}^{\mathrm{i}\left(\varphi_{x2}-2\theta_2\right)}\right] \equiv 0 \\ H-J = \dfrac{\mathrm{i}B-A}{4}\cdot\left[\mathrm{e}^{\mathrm{i}\left(\varphi_{x1}+2\theta_1\right)} + \mathrm{e}^{\mathrm{i}\left(\varphi_{x2}+2\theta_2\right)}\right] \equiv 0 \end{cases}. \tag{13}$$

Equations (12) and (13) are exploited to engender RCP and LCP waves at the focal plane, respectively. Here, we discuss the situation where the metasurface zone plate generates RCP waves at the focal plane under nearly arbitrary polarization incidence. After careful calculations, we have obtained a set of solutions to Eq. (12): $\varphi_{x1} = \theta_1 = 0$, $\varphi_{x2} = 3\pi/2$ and $\theta_2 = \pi/4$. In the same way as in Section *Linear polarizer with focusing function*, the CST microwave studio is utilized to determine the suitable meta-atoms which are depicted in Fig. 4(a) and 4(b). These two types of meta-atoms are defined as Meta-atom 1 and Meta-atom 2, respectively. For Meta-atom 1, its period, length and width correspond to P = 150 μm, L_1 = 118 μm and W_1 = 50 μm. While the Meta-atom 2 is obtained by rotating a rectangular silicon pillar with length of L_2 = 48 μm and width of W_2 = 78 μm along the +x axis by π/4. Figure 4(c) (Fig. 4(e)) plots the relationship between the amplitudes of the CP components generated by the designed meta-atoms and the incident frequency, under LCP (RCP) incidence. Obviously, when the frequency of the incident CP wave is 1 THz, the amplitude of the co-polarized component of the outgoing wave is almost zero, demonstrating that the outgoing wave is a cross-polarized wave. Figure 4(d) shows the

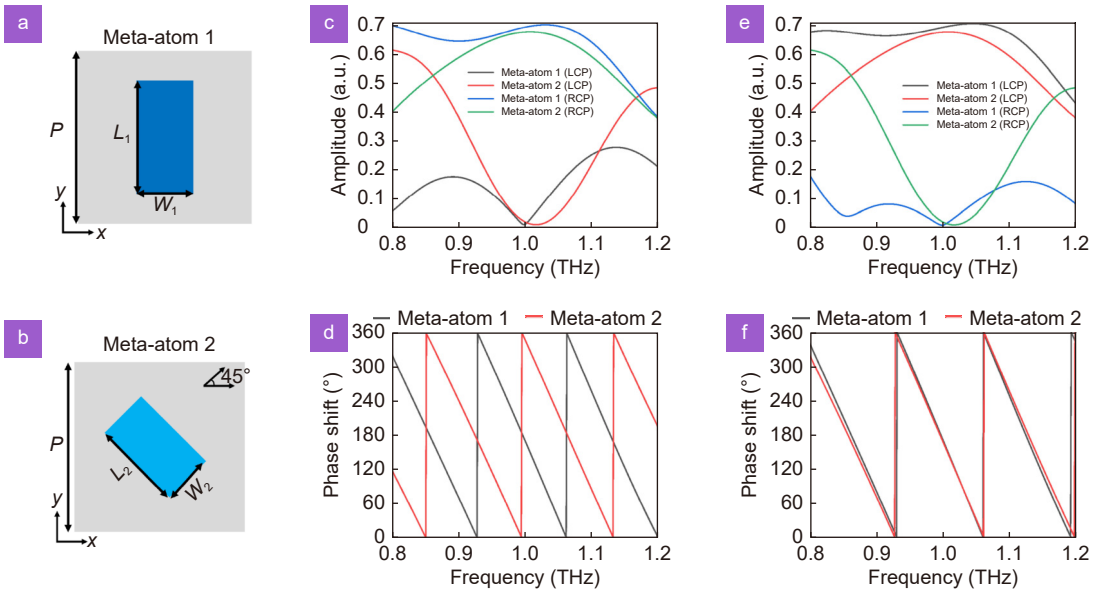

Fig. 4 | (**a**) Schematic of the Meta-atom 1. (**b**) Top view of the Meta-atom 2. (**c**) Transmission amplitudes of cross- and co-polarized components at different frequencies, under LCP incidence. (**d**) Simulated results of phase shifts under LCP incidence. (**e**) The relationship between the transmission amplitudes of the orthogonal CP components and the incident frequency, when the RCP wave is incident. (**f**) The phase shift of the transmitted LCP wave at different incident frequencies under RCP incidence.

phase shift of cross-polarized waves in response to different incident frequencies under LCP illumination, while the relationship between the phase shift of the transmitted LCP component and incident frequency under RCP incidence is plotted in Fig. 4(f). For LCP incidence, the phase difference between the phase shifts generated by Meta-atom 1 and Meta-atom 2 is π at 1 THz, which can be seen from Fig. 4(d). For RCP incidence, the phase shifts of the transmitted waves generated by these two meta-atoms are equal (see Fig. 4(f)).

With this, the Meta-atom 1 and Meta-atom 2 are utilized as the basic unit to construct the even-numbered and odd-numbered ring zones in the metasurface zone plate, respectively. Figure 5(a) shows a cross-sectional view of the metasurface wave zone plate designed based on the above concept. Figure 5(b) and 5(c) illustrate the simulated intensity profiles of the focal plane under LCP and RCP incidence, respectively, whose inset is the

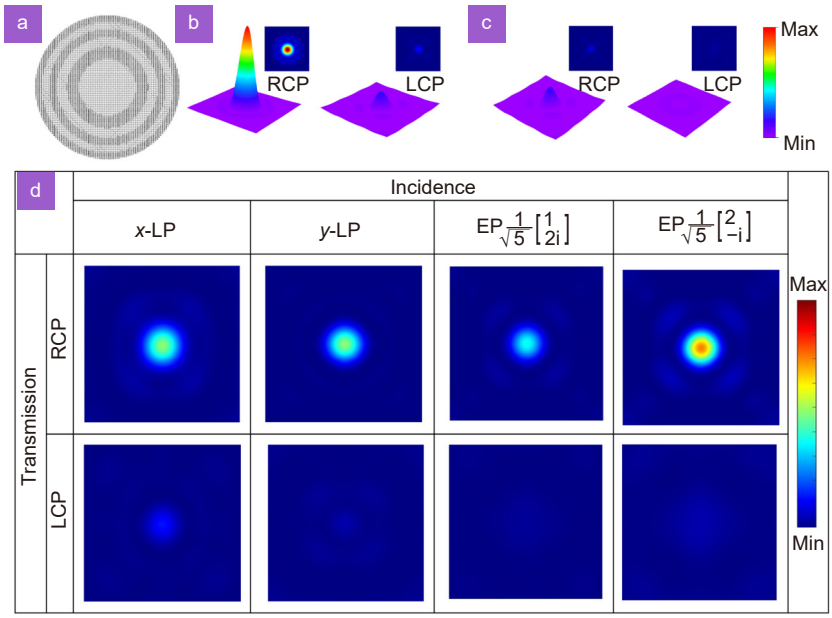

Fig. 5 | (**a**) Schematic diagram of the structure of the metasurface zone plate. (**b**, **c**) The intensity distributions of the cross- and co-polarized components at the focal plane under CP incidences. (**d**) The simulated intensity distribution of the focal plane under LP and EP incidences.

corresponding two-dimensional display. Comparing Fig. 5(b) and 5(c), it can be found that the designed metasurface zone plate can generate RCP waves at the focus under LCP incidence, but cannot engender any outgoing waves at the focus under RCP incidence, that is to say, the metasurface zone plate has a chiro-optical response. It is worth noting that the polarization conversion ratio is a crucial parameter to measure the polarizer, which can be expressed as PCR= $P_R/(P_R+P_L)$, where P_R is the power of the transmitted RCP component and P_L is the power of the LCP. Through simulated calculation, we obtain that the polarization conversion ratio is 89.12% under LCP incidence, indicating such a metasurface zone plate has an efficient polarization conversion ratio. Moreover, the simulated results in response to other incident polarized waves are shown in Fig. 5(d). Obviously, under LP or EP incidence, the outgoing wave on the focal plane generated by the metasurface zone plate keeps as the RCP wave throughout.

Next, the sample is fabricated exploiting the same etching technique as in Section *Linear polarizer with focusing function*, whose corresponding SEM image is shown in Fig. 6(a). The intensity distributions (see Fig. 6(b)) of different polarized components are obtained by changing the polarization state of the incident wave in the imaging system. It can be seen that the experimental results in Fig. 6 are consistent with the simulated results in Fig. 5: once the polarization state of the incident wave is not right-handed circular polarization, the outgoing wave at the focusing plane is the RCP wave. In short, the results of experiments and simulations manifest that the fixed polarization conversion can be effectively achieved via the metasurface zone plate.

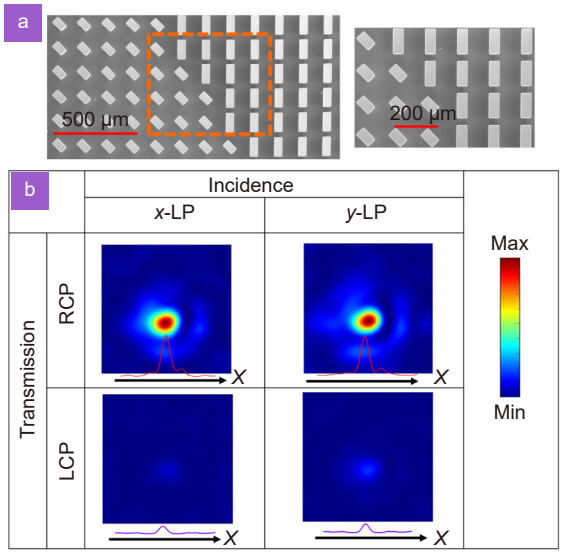

Fig. 6 | (**a**) SEM image of the fabricated metasurface zone plate. (**b**) The measured intensity profiles of the focal plane under CP and LP incidences. The inset is the intensity distribution across the focus along the x-axis.

Conclusions

In conclusion, we introduce the Fresnel zone plate into the metasurface to construct the metasurface zone plate, which can convert nearly arbitrary polarizations into a fixed polarization. As demonstrations, in the designed metasurface zone plates, the odd-numbered and even-numbered ring zones, which can be regarded as independent regions, are composed of different meta-atoms. Arbitrarily polarized beams incident on the metasurface zone plates will generate the outgoing wave which are superimposed at the focal plane to form a *x*-LP or RCP beam. The feasibility and practicability of such design scheme are verified by theory, simulation and experiment. We firmly believe that this strategy can effectively reduce the difficulty of fabricating polarized generators and may improve the versatility and integration of optical devices

References

1. Zijlstra P, Chon JWM, Gu M. Five-dimensional optical recording mediated by surface plasmons in gold nanorods. *Nature* **459**, 410–413 (2009).
2. Li XP, Lan TH, Tien CH, Gu M. Three-dimensional orientation-unlimited polarization encryption by a single optically configured vectorial beam. *Nat Commun* **3**, 998 (2012).
3. Wang JY, Tan XD, Qi PL, Wu CH, Huang L et al. Huang L et al. Linear polarization holography. *Opto-Electron Sci* **1**, 210009 (2022).
4. Scheel S, Welsch DG. Quantum theory of light and noise polarization in nonlinear optics. *Phys Rev Lett* **96**, 073601 (2006).
5. Liu J, Shi MQ, Chen Z, Wang SM, Wang ZL et al. Quantum photonics based on metasurfaces. *Opto-Electron Adv* **4**, 200092 (2021).
6. Stav T, Faerman A, Maguid E, Oren D, Kleiner V et al. Quantum entanglement of the spin and orbital angular momentum of photons using metamaterials. *Science* **361**, 1101–1103 (2018).
7. Li JT, Wang GC, Yue Z, Liu JY, Li J et al. Dynamic phase assembled terahertz metalens for reversible conversion between linear polarization and arbitrary circular polarization. *Opto-Electron Adv* **5**, 210062 (2022).
8. Rubin NA, D'Aversa G, Chevalier P, Shi ZJ, Chen WT et al. Matrix Fourier optics enables a compact full-Stokes polarization camera. *Science* **365**, eaax1839 (2019).
9. Gansel JK, Thiel M, Rill MS, Decker M, Bade K et al. Gold helix photonic metamaterial as broadband circular polarizer. *Science* **325**, 1513–1515 (2009).
10. Kim TT, Oh SS, Kim HD, Park HS, Hess O et al. Electrical access to critical coupling of circularly polarized waves in graphene chiral metamaterials. *Sci Adv* **3**, e1701377 (2017).
11. Li W, Coppens ZJ, Besteiro LV, Wang WY, Govorov AO et al.

Circularly polarized light detection with hot electrons in chiral plasmonic metamaterials. *Nat Commun* **6**, 8379 (2015).
12. Ma W, Cheng F, Liu YM. Deep-learning-enabled on-demand design of chiral metamaterials. *ACS Nano* **12**, 6326–6334 (2018).
13. Pfeiffer C, Zhang C, Ray V, Guo LJ, Grbic A. High performance bianisotropic metasurfaces: asymmetric transmission of light. *Phys Rev Lett* **113**, 023902 (2014).
14. Turner MD, Saba M, Zhang QM, Cumming BP, Schröder-Turk GE et al. Miniature chiral beamsplitter based on gyroid photonic crystals. *Nat Photonics* **7**, 801–805 (2013).
15. Tanaka K, Arslan D, Fasold S, Steinert M, Sautter J et al. Chiral bilayer all-dielectric metasurfaces. *ACS Nano* **14**, 15926–15935 (2020).
16. Zhang Y B, Liu H, Cheng H, Tian J G, Chen S Q. Multidimensional manipulation of wave fields based on artificial microstructures. *Opto-Electron Adv* **3**, 200002 (2020).
17. Lee HE, Ahn HY, Mun J, Lee YY, Kim M et al. Amino-acid- and peptide-directed synthesis of chiral plasmonic gold nanoparticles. *Nature* **556**, 360 (2018).
18. Mun J, Kim M, Yang Y, Badloe T, Ni JC et al. Electromagnetic chirality: from fundamentals to nontraditional chiroptical phenomena. *Light-Sci Appl* **9**, 139 (2020).
19. Mun J, Rho J. Surface-enhanced circular dichroism by multipolar radiative coupling. *Opt Lett* **43**, 2856–2859 (2018).
20. Yang Y, Kim M, Mun J, Rho J. Ultra-sharp circular dichroism induced by twisted layered C4 oligomers. *Adv Theor Simul* **3**, 1900229 (2020).
21. Zhang S, Zhou JF, Park YS, Rho J, Singh R et al. Photoinduced handedness switching in terahertz chiral metamolecules. *Nat Commun* **3**, 942 (2012).
22. Ye WM, Yuan XD, Guo CC, Zhang JF, Yang B et al. Large chiroptical effects in planar chiral metamaterials. *Phy Rev A* **7**, 054003 (2017).
23. Ma ZJ, Li Y, Li Y, Gong YD, Maier SA et al. All-dielectric planar chiral metasurface with gradient geometric phase. *Opt Express* **26**, 6067–6078 (2018).
24. Zheng CL, Li J, Wang SL, Li JT, Li MY et al. Optically tunable all-silicon chiral metasurface in terahertz band. *Appl Phys Lett* **118**, 051101 (2021).
25. Yue Z, Zheng CL, Li J, Li JT, Liu JY et al. A dual band spin-selective transmission metasurface and its wavefront manipulation. *Nanoscale* **13**, 10898–10905 (2021).
26. Li JT, Li J, Zheng CL, Wang SL, Li MY et al. Dynamic control of reflective chiral terahertz metasurface with a new application developing in full grayscale near field imaging. *Carbon* **172**, 189–199 (2021).
27. Li J, Li JT, Yang Y, Li JN, Zhang YT et al. Metal-graphene hybrid active chiral metasurfaces for dynamic terahertz wavefront modulation and near field imaging. *Carbon* **163**, 34–42 (2020).
28. Fedotov VA, Mladyonov PL, Prosvirnin SL, Rogacheva AV, Chen Y et al. Asymmetric propagation of electromagnetic waves through a planar chiral structure. *Phys Rev Lett* **97**, 167401 (2006).
29. Khaliq HS, Kim I, Kim J, Oh DK, Zubair M et al. Manifesting simultaneous optical spin conservation and spin isolation in diatomic metasurfaces. *Adv Opt Mater* **9**, 2002002 (2021).
30. Zhang F, Pu MB, Li X, Gao P, Ma XL et al. All-dielectric metasurfaces for simultaneous giant circular asymmetric transmission and wavefront shaping based on asymmetric photonic spin-orbit interactions. *Adv Funct Mater* **27**, 1704295 (2017).
31. Zheng CL, Li J, Li JT, Yue Z, Wang SL et al. All-silicon chiral metasurfaces and wavefront shaping assisted by interference. *Sci China Phys Mech Astron* **64**, 114212 (2021).
32. Rana AS, Kim I, Ansari MA, Anwar MS, Saleem M et al. Planar achiral metasurfaces-induced anomalous chiroptical effect of optical spin isolation. *ACS Appl Mater Interfaces* **12**, 48899–48909 (2020).
33. Gao S, Zhou CY, Yue WJ, Li Y, Zhang CW et al. Efficient all-dielectric diatomic metasurface for linear polarization generation and 1-Bit phase control. *ACS Appl Mater Interfaces* **13**, 14497–14506 (2021).
34. Li ZC, Liu WW, Cheng H, Choi DY, Chen SQ et al. Arbitrary manipulation of light intensity by bilayer aluminum metasurfaces. *Adv Opt Mater* **7**, 1900260 (2019).
35. Zhang YL, Cheng Y, Chen M, Xu RH, Yuan LB. Ultracompact metaimage display and encryption with a silver nanopolarizer based metasurface. *Appl Phys Lett* **117**, 021105 (2020).
36. Li X, Tang J, Baine J. Polarization-independent metasurface lens based on binary phase fresnel zone plate. *Nanomaterials* **10**, 1467 (2020).
37. Wang JY, Yang JQ, Kang GG. Achromatic focusing effect of metasurface-based binary phase Fresnel zone plate. *Phys Lett A* **407**, 127463 (2021).
38. Yoon G, Jang J, Mun J, Nam KT, Rho J. Metasurface zone plate for light manipulation in vectorial regime. *Commun Phys* **2**, 156 (2019).
39. Yang BW, Liu T, Guo HJ, Xiao SY, Zhou L. High-performance meta-devices based on multilayer meta-atoms: interplay between the number of layers and phase coverage. *Sci Bull* **64**, 823–835 (2019).
40. Huang WX, Lin J, Qiu M, Liu T, He Q et al. A complete phase diagram for dark-bright coupled plasmonic systems: applicability of Fano's formula. *Nanophotonics* **9**, 3251–3262 (2020).
41. Li Y, Lin J, Guo HJ, Sun WJ, Xiao SY et al. A tunable metasurface with switchable functionalities: from perfect transparency to perfect absorption. *Adv Opt Mater* **8**, 1901548 (2020).
42. Zhang XY, Li Q, Liu FF, Qiu M, Sun SL et al. Controlling angular dispersions in optical metasurfaces. *Light-Sci Appl* **9**, 76 (2020).

Acknowledgements

We are grateful for financial supports from the National Key Research and Development Program of China (Nos. 2021YFB2800703 and 2017YFA0700202), and the National Natural Science Foundation of China (Nos. 61675147, 61735010 and 91838301).

Author contributions

Z. Yue: conceptualization, methodology, writing-original draft preparation; J. T. Li, J. Li and C. L. Zheng: software, data curation, revision; J. Y. Liu, G. C. Wang and H. Xu: software, visualization, investigation; M. Y. Chen, Y. T. Zhang, Y. Zhang and J. Q. Yao: supervision, reviewing.

Competing interests

The authors declare no competing financial interests.

Supplementary information

Supplementary information for this paper is available at https://doi.org/10.29026/oes.2022.210014